ACS chemical biology

Articles

pubs.acs.org/acschemicalbiology

Mapping Novel Metabolic Nodes Targeted by Anti-Cancer Drugs that Impair Triple-Negative Breast Cancer Pathogenicity

Lindsay S. Roberts, Peter Yan, Leslie A. Bateman, and Daniel K. Nomura*

Departments of Chemistry, Molecular and Cell Biology, and Nutritional Sciences and Toxicology, 127 Morgan Hall, University of California, Berkeley, Berkeley, California 94720, United States

Supporting Information

ABSTRACT: Triple-negative breast cancers (TNBCs) are estrogen receptor, progesterone receptor, and HER2 receptor-negative subtypes of breast cancers that show the worst prognoses and lack targeted therapies. Here, we have coupled the screening of ∼400 anticancer agents that are under development or in the clinic with chemoproteomic and metabolomic profiling to identify novel metabolic mechanisms for agents that impair TNBC pathogenicity. We identify 20 anticancer compounds that significantly impaired cell survival across multiple types of TNBC cells. Among these 20 leads, the phytoestrogenic natural product licochalcone A was of interest, since TNBCs are unresponsive to estrogenic therapies, indicating that licochalcone A was likely acting through another target. Using chemoproteomic profiling approaches, we reveal that licochalcone A impairs TNBC pathogenicity, not through modulating estrogen receptor activity but rather through inhibiting prostaglandin reductase 1, a metabolic enzyme involved in leukotriene B4 inactivation. We also more broadly performed metabolomic profiling to map additional metabolic mechanisms of compounds that impair TNBC pathogenicity. Overlaying lipidomic profiling with drug responses, we find that deubiquitinase inhibitors cause dramatic elevations in acyl carnitine levels, which impair mitochondrial respiration and contribute to TNBC pathogenic impairments. We thus put forth two unique metabolic nodes that are targeted by drugs or drug candidates that impair TNBC pathogenicity. Our results also showcase the utility of coupling drug screens with chemoproteomic and metabolomic profiling to uncover unique metabolic drivers of TNBC pathogenicity.

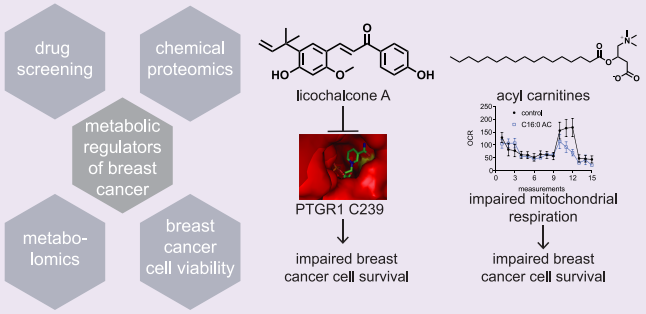

In the United States, it is estimated that over 200 000 women will be diagnosed with breast cancer and nearly 40 000 women will die of breast cancer in 2016.[1] Mortality from breast cancer is almost always attributed to metastatic spread of the disease to other organs, thus precluding resection as a treatment method.[2] Unfortunately, conventional chemotherapy fails to eradicate many aggressive breast cancers.[2] Studies over the past decade have uncovered certain breast cancer cell-types, such as estrogen/progesterone/HER2 receptor (ER/PR/HER2)-negative (triple-negative) breast cancers (TNBCs) that show poor prognosis and chemotherapy resistance within breast tumors.[3−5] Eliminating these breast cancer types is critical in reducing the mortality associated with breast cancer.

Current therapeutic strategies for breast cancer include resection, nonspecific therapies such as radiation or chemotherapy, and targeted strategies for combating certain types of breast cancers.[6] However, there are no targeted strategies for combating the most aggressive types of breast cancers, including TNBCs. Since the discoveries of Otto Warburg in the 1920s showing that cancer cells are addicted to glucose metabolism, we have known that cancer cells possess fundamentally altered metabolism that drives nearly every aspect of their pathogenicity.[7] The past decade has seen a resurgence of interest in targeting metabolic drivers of cancer for therapy. As such, many metabolic pathways, targets, and inhibitors have been discovered for potential cancer therapy, including pyruvate kinase activators that target glycolytic metabolism, isocitrate dehydrogenase mutant-specific inhibitors that impair oncometabolite synthesis, fatty acid synthase inhibitors that impair lipogenesis, and phosphoglycerate dehydrogenase inhibitors that target serine metabolism. These targets and pathways are likely just the tip of the iceberg in terms of potential metabolic targets and pathways that may be exploited for cancer therapy.

In this study, we hoped to discover new strategies to impair TNBC pathogenicity. We combined chemoproteomic and metabolomic profiling to elucidate protein targets and metabolic effects of known anticancer drugs. Through this profiling effort, we have uncovered novel metabolic mechanisms and anti-TNBC activities of the phytoestrogenic natural product licochalcone A and deubiquitinase inhibitors.

Received: December 30, 2016
Accepted: March 1, 2017
Published: March 1, 2017

DOI: 10.1021/acschembio.6b01159
ACS Chem. Biol. XXXX, XXX, XXX−XXX

RESULTS AND DISCUSSION

To discover drugs and drug candidates that impair TNBC pathogenicity, we screened an anticancer library consisting of 424 compounds spanning a diverse range of molecular targets to identify small-molecules that impaired serum-free cell survival in 231MFP and HCC38 TNBC cells (Figure S1, Figure 1, Table S1). We then filtered this list for those

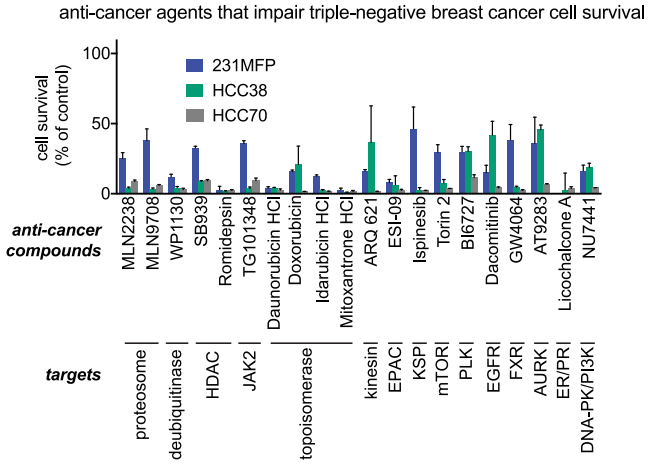

Figure 1. Screening a library of anticancer drugs and drug candidates in TNBC cells. A library of anticancer drugs and drug candidates were screened in 231MFP and HCC38 TNBC cell lines for impairments in serum-free cell survival. This data are shown in Figure S1 and Table S1. Shown here are drugs and drug candidates that reproducibly and significantly impaired 231MFP, HCC38, and HCC70 serum-free cell survival by >50%. Cells were treated with DMSO vehicle or compound (10 μM) in serum-free media, and cell survival was assessed 48 h after treatment by Hoescht staining. Data are presented as mean ± SEM, n = 3/group, and all compounds shown in this figure showed significant (p < 0.05) cell survival impairments compared to DMSO-treated controls.

compounds that showed >75% survival impairments in both 231MFP and HCC38 cells. We subsequently retested the filtered list of compounds to identify agents that significantly (p < 0.05) impaired cell survival across 231MFP, HCC38, and HCC70 TNBC cells by over 50%. This resulted in a list of 20 compounds spanning 15 different molecular targets that reproducibly and significantly impaired cell survival by >50% across three TNBC lines (Figure 1).

Several of these 20 compounds inhibit proteins that are currently being targeted in TNBC patients or are in clinical development including proteasome inhibitors MLN2238 and MLN9708; topoisomerase inhibitors daunorubicin, doxorubicin, idarubicin, and mitoxantrone; JAK2 inhibitor TG101348; mTOR inhibitor Torin 2; EGFR inhibitor dacomitinib; polo-like kinase 1 (PLK) inhibitor BI6727; kinesin spindle protein (KSP) inhibitor ispenisib; and aurora kinase (AURK) inhibitor AT9283.[4,8−13] Other compounds modulate protein targets that have been previously shown to be important in TNBCs including HDAC inhibitors SB939 and romidepsin.[14] The remaining compounds and their targets, while previously shown to be important in cancer, are less understood in regard to their efficacy or roles in advanced-stage breast cancers or TNBCs. These include deubiquitinase inhibitor WP1130, exchange proteins directly activated by cAMP isoform 1 (EPAC) inhibitor ESI-09, kinesin inhibitor ARQ 621, FXR activator GW4064, and the phytoestrogen natural product licochalcone A[15−19] and may represent promising therapeutic strategies for combating TNBCs. Among these compounds with poorly understood roles in TNBCs, licochalcone A showed the greatest impairment (>95%) in cell survival across the three TNBC cells tested here with a 50% effective concentration (EC50) of 8.4 μM (Figure S2).

The target of licochalcone A is the estrogen or progesterone receptor based on previous characterization of this compound as an estrogenic flavonoid.[17] Licochalcone A is a flavonoid extracted from licorice root that has been shown to possess anticancer, anti-inflammatory, and antiparasitic activity and has been tested on humans as an anti-inflammatory moisturizer.[17,20−25] However, the cell survival impairments of licochalcone A in TNBC cells resistant to ER and PR signaling indicated that this compound may be acting through alternate targets.

Licochalcone A belongs to a larger group of natural products known as chalcones characterized by their aromatic enone structures (Figure 2A). These enones can undergo Michael addition to cysteine thiols on proteins to modulate protein function.[26] To identify the potential anticancer targets of licochalcone A, we mapped the cysteine reactivity of this compound in TNBC cells using a chemoproteomic platform termed isotopic tandem orthogonal proteolysis-enabled activity-based protein profiling (isoTOP-ABPP). IsoTOP-ABPP uses reactivity-based probes to map proteome-wide reactive, functional, and ligandable hotspots directly in complex proteomes. When used in a competitive manner, small molecules like licochalcone A can be competed against reactivity-based probes to map the proteome-wide reactivity and targets of covalently acting compounds (Figure 2B).[27−29] We profiled the proteome-wide cysteine-reactivity of licochalcone A through competition of this agent against the broad cysteine-reactive iodoacetamide-alkyne probe in 231MFP proteomes using the isoTOP-ABPP platform.[27,30] We subsequently appended probe-labeled proteins with a biotin-azide handle bearing an isotopically light (for control) or heavy (for licochalcone-treated) mass tag bearing a TEV protease recognition sequence by copper-catalyzed azide−alkyne cycloaddition (CuAAC), followed by mixing vehicle-treated and licochalcone-treated proteomes in a 1:1 ratio, avidin enrichment of probe-labeled proteins, digestion of enriched proteins by trypsin, and subsequent isolation and elution of probe-modified tryptic peptides by TEV protease for subsequent quantitative proteomic analysis of light to heavy peptide ratios (Figure 2B). Through this profiling effort, we identified 1410 probe-modified tryptic peptides that were present in at least two out of four biological replicates (Figure 2C; Table S2). Most peptides showed light to heavy isotopic ratios of ∼1, indicating that most sites were not inhibited. We interpreted those sites that showed light to heavy isotopic ratios >10 as true targets of licochalcone A (Figure 2C; Table S2).

From this study, we found the primary target of licochalcone A to be cysteine 239 of the metabolic enzyme target prostaglandin reductase 1 (PTGR1) with the highest isotopic light to heavy ratio of 27 (Figure 2C; Table S2). We validated this target using gel-based ABPP methods where we observed competition of licochalcone A against iodoacetamide-alkyne labeling of pure human PTGR1 protein (Figure 2C). PTGR1 is involved in inactivating prostaglandins, including 15-keto-prostaglandins and leukotriene B4.[31] While recently shown to be important in lung and prostate cancers, PTGR1 represents a novel target for breast cancer.[32,33] Leukotriene B4, through

DOI: 10.1021/acschembio.6b01159
ACS Chem. Biol. XXXX, XXX, XXX−XXX

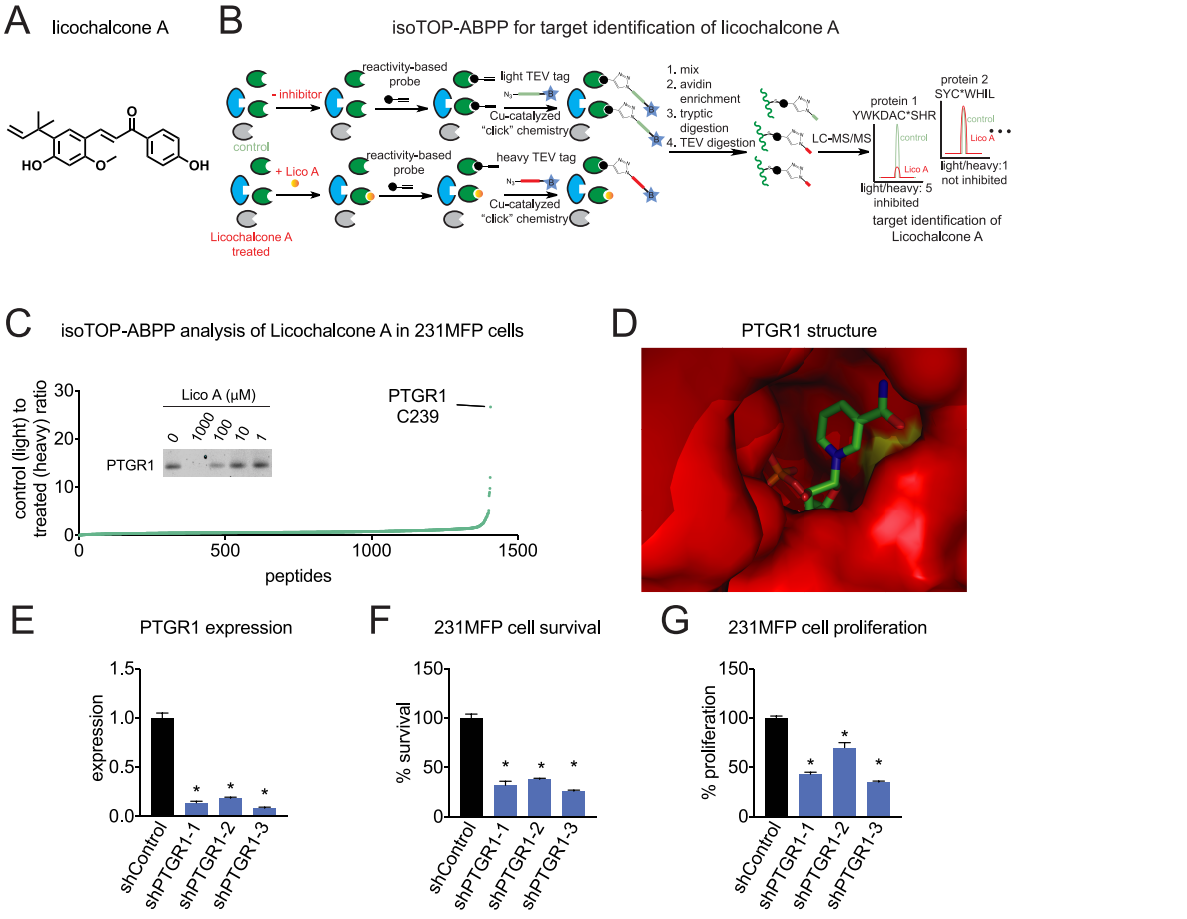

Figure 2. IsoTOP-ABPP analysis of licochalcone A in TNBC cells. (A) Structure of licochalcone A. (B) Competitive isoTOP-ABPP to map licochalcone targets. Licochalcone A bears a Michael acceptor that is potentially cysteine-reactive. We mapped the cysteine-reactivity of licochalcone A by preincubating licochalcone A (10 μM) for 30 min in 231MFP breast cancer cell proteomes, prior to labeling with the cysteine-reactive iodoacetamide-alkyne (IAyne) probe (100 μM, 30 min). Probe labeled proteins were then tagged with an isotopically light (for control) or heavy (for licochalcone A-treated) biotin-azide tag bearing a TEV protease recognition site by CuAAC. Control and treated proteomes were then mixed in a 1:1 ratio. Probe labeled proteins were avidin-enriched and tryptically digested. Probe-labeled tryptic peptides were avidin-enriched again and released by TEV protease and analyzed by quantitative proteomic methods, and light to heavy peptide ratios were quantified. (C) Competitive isoTOP-ABPP analysis of licochalcone A cysteine reactivity in 231MFP breast cancer cell proteomes. Light to heavy ratios of ~1 indicate peptides that were labeled by IAyne, but not bound by licochalcone A. We designate light to heavy ratios of >10 as targets that were bound by licochalcone A. The top target was C239 of PTGR1. Shown in this figure is also validation of PTGR1 as a target of licochalcone A. Licochalcone A was preincubated with pure human PTGR1 protein followed by IAyne. Probe-labeled proteins conjugated to rhodamine-azide by CuAAC and analyzed by SDS/PAGE and in-gel fluorescence. Shown are average isotopic ratios of probe-modified tryptic peptides that were present in at least two out of four biological replicates. (D) Crystal structure of PTGR1 showing C239 (shown in yellow) and NADP+ shown in ball and stick form. PDB structure used is 2Y05. (E) PTGR1 expression in shPTGR1 231MFP cells. PTGR1 was stably knocked down with three independent shRNA oligonucleotides, and expression was determined by qPCR. (F, G) Serum-free cell survival and proliferation in shPTGR1 231MFP cells. Cell survival and proliferation were assessed 48 h after seeding by Hoescht staining. Data in E−G are presented as mean ± SEM, n = 3−5/group. Significance is presented as *p < 0.05 compared to shControl cells.

stimulating leukotriene B4 receptor BLT1, has also been shown to fuel TGF-β−mediated proliferation in breast cancer cells.[34] Interestingly, C239 of PTGR1 represents the binding region for NADP+, required for the reductase catalytic activity of this enzyme[35] (Figure 2D), suggesting that licochalcone A binding to this site would displace NADP+ binding and inhibit PTGR1 activity. To further confirm the importance of PTGR1 in TNBC pathogenicity, we knocked down the expression of PTGR1 in 231MFP TNBC cells using three independent short-hairpin RNA oligonucleotides and show that PTGR1 knock-down dramatically impairs 231MFP cell survival and proliferation, thus recapitulating the effects observed with licochalcone A (Figure 2E−G). Thus, we put forth a novel metabolic mechanism of licochalcone A, in which it inhibits PTGR1 to impair TNBC pathogenicity.

We next sought to take a broader approach toward identifying unique metabolic mechanism underlying agents that impair TNBC pathogenicity. We performed lipidomic profiling to map metabolic changes conferred by treatment of 231MFP TNBC cells with the 20 lead compounds that impaired TNBC cell survival (Figure 3A; Table S3). We focused this study on measuring ~100 lipid metabolites spanning phospholipids, fatty acids, neutral lipids, sphingolipids, sterols, and fatty acid derivatives such as acyl carnitines, N-acyl ethanolamines (NAEs), and N-acyl taurines (NATs). We performed lipidomic profiling on cells that were treated for 6 h before any cell death to avoid confounding effects that may arise from differing cell numbers. Interestingly, we find that each compound gives a unique lipidomic signature, suggesting that metabolomic profiling may be used as a potential

DOI: 10.1021/acschembio.6b01159
ACS Chem. Biol. XXXX, XXX, XXX−XXX

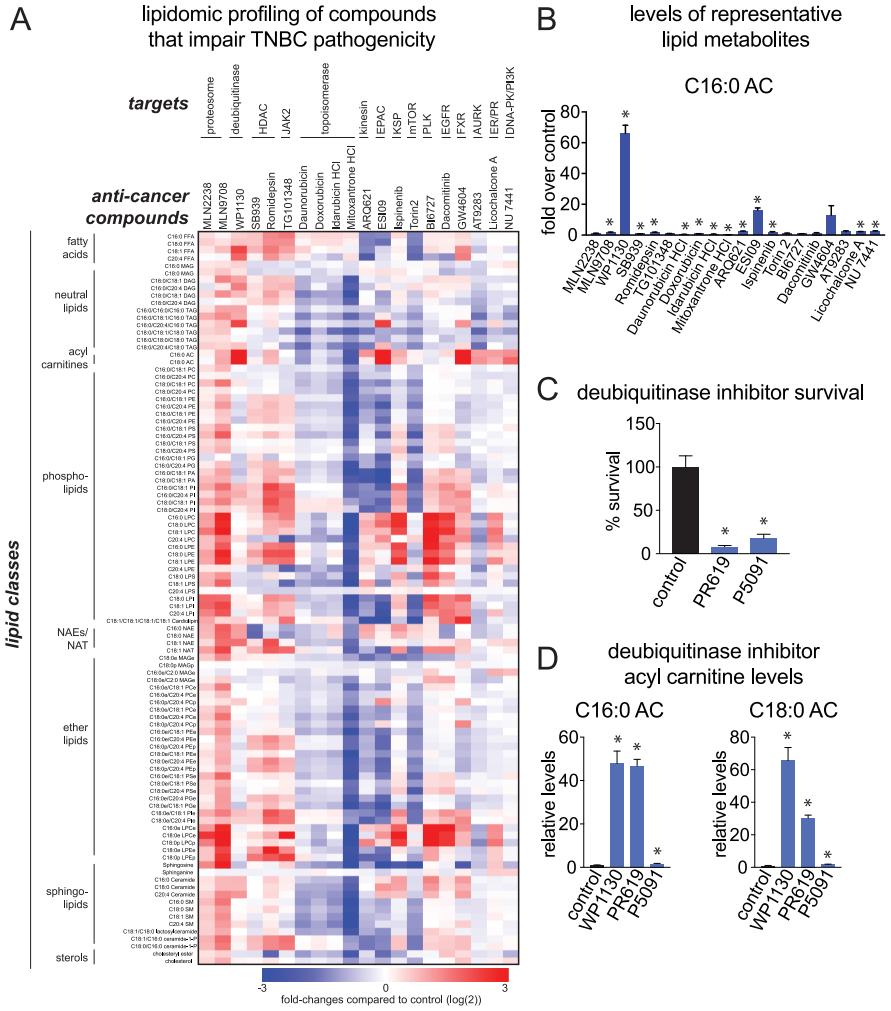

Figure 3. Metabolomic profiling of drug responses in TNBC cells. (A) Metabolomic profiling of 231MFP TNBC cells treated with the 20 compounds that impaired TNBC cell survival. 231MFP cells were treated with DMSO vehicle or each compound (10 μM) for 6 h. Lipid levels were analyzed by single reaction monitoring (SRM)-based liquid chromatography−mass spectrometry (LC-MS/MS). Heatmap shows fold changes in log (2) compared to vehicle-treated controls where red and blue designates increased and decreased levels, respectively. (B) C16:0 AC levels in 231MFP cells treated with each of the 20 compounds that impaired TNBC cell survival. Data are from the experiment described in A. (C) Cell survival in 231MFP cells. 231MFP cells were treated with DMSO control or deubiquitinase inhibitors PR619 and P5091 (10 μM), and serum-free cell survival was assessed 48 h after treatment by Hoescht staining. (D) AC levels in 231MFP cells treated with deubiquitinase inhibitors. Cells were treated with DMSO vehicle or inhibitors (10 μM) for 6 h, and AC levels were determined by SRM-based LC-MS/MS. Data in A are from an n = 5/group. Data in B−D are presented as mean ± SEM, n = 5/group. Significance is presented as *p < 0.05 compared to vehicle-treated control cells.

biomarker of drug response (Figure 3A; Figure S3; Table S3). We also see common changes in specific metabolites that correlate with certain mechanisms of action. For example, we observe that topoisomerase inhibitor-treated cells show reduced levels of C18:0/C18:1 diacylglycerol (DAG) and C18:0 ceramide, not seen with most of the other drug treatments, potentially indicating that these lipid species may be more specifically controlled by topoisomerase-mediated pathways (Figure S3; Table S3). We also see certain lipid classes that are similarly regulated by multiple drugs that do not necessarily share a common mechanism of action. For example, C16:0 and C18:0 lysphosphatidylethanolamines (LPE), C16:0 lysophosphatidylcholine (LPC), and C18:0e lysophosphatidylcholine-ether (LPCe) levels are significantly elevated upon treatment of 231MFP cells with proteasome inhibitors MLN2238 and MLN9708, HDAC inhibitor romidepsin, JAK2 inhibitor TG101348, KSP inhibitor ispinenib, PLK inhibitor BI6727, EGFR inhibitor dacomitinib, and licochalcone A (Figure S3; Table S3). Perhaps this common regulation of different types of lysophospholipids by compounds that act through different targets may suggest a common downstream pathway targeted across all of these mechanisms—potentially through an activation of phospholipase enzymes that would generate lysophospholipids. We do not believe these lipidomic signatures to be a general signature of cell death, as all 20 of these drugs impair TNBC cell survival. Rather, we believe that these lipidomic signatures likely represent unique metabolic mechanisms underlying the action of each drug.

Among the lipidomic profiles, the most significant changes were in acyl carnitine (AC) levels with a >60-fold elevation in C16:0 AC with the deubiquitinase inhibitor WP1130 and a >10-fold elevation with the EPAC inhibitor ESI09 and FXR activator GW4604 (Figure 3B; Table S3). ACs are metabolites generated by carnitine palmitoyltranferase 1 (CPT1) at the mitochondrial membrane to import fatty acids into the mitochondria for fatty acid oxidation.[36] We show that other deubiquitinase inhibitors PR619 and P5091 also impair 231MFP cell survival and elevate AC levels (Figure 3C,D).

DOI: 10.1021/acschembio.6b01159
ACS Chem. Biol. XXXX, XXX, XXX−XXX

While PR619 and WP1130 inhibit several deubituitinases, P5091 selectively inhibits USP7 and USP47, which may explain the less dramatic AC elevations with P5091. We show that AC treatment impairs cell survival (Figure 4A). We also find that

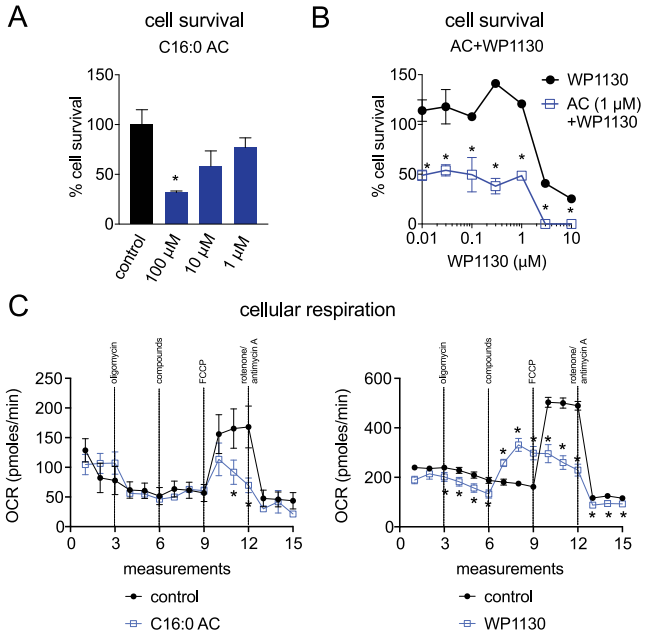

Figure 4. The role of AC in deubiquitinase inhibitor-mediated cell survival impairments in TNBC cells. (A) 231MFP cell survival upon treatment of cells with AC. Cells were treated with AC, and serum-free cell survival was assessed 48 h after treatment by Hoescht staining. (B) 231MFP cell survival upon treatment of cells with AC and deubiquitinase inhibitor WP1130. Cells were cotreated with water or C16:0 AC (1 μM) at a concentration that does not impair viability when treated alone and DMSO or WP1130, and cell survival was assessed 48 h after treatment by Hoescht staining. (C) Oxygen consumption rates in cells treated with DMSO vehicle or AC or WP1130. Compounds were treated at cycle 6 (injection from port B). Oxygen consumption was measured using a Seahorse XF24 Analyzer. Data in A–C are presented as mean ± SEM, n = 3–5/group. Significance is presented as $^*p < 0.05$ compared to vehicle-treated control cells.

treatment of 231MFP cells with a concentration of AC that does not impair cell survival dramatically sensitizes cells to WP1130, likely because AC treatment synergizes with WP1130-mediated elevations in AC to impair 231MFP viability (Figure 4B). Previous studies have shown that ischemic injury elevates the levels of AC and that AC uncouples the mitochondria and impairs cellular respiration.[37−39] We show that treatment of 231MFP cells with both AC and WP1130 impairs maximal cellular respiration to a comparable degree (Figure 4C). Our data thus suggest that inhibition of deubiquitinase enzymes leads to elevation in AC levels which, in turn, impair cellular respiration and may contribute to the cell survival impairments.

We also tested the role of LPE, since lysophospholipid species were among the lipid species dramatically changed with several drugs. We show that LPE treatment also impairs 231MFP cell survival and potentiates the cell survival impairments conferred by the proteasome inhibitor MLN9708 that elevates LPE levels (Figures S3, S4). We further demonstrate that, unlike AC treatment, LPE or palmitate treatment in 231MFP cells does not affect cellular respiration, indicating that the lysophospholipid effects are driven through an alternate mechanism (Figure S4).

In summary, we reveal several unique and novel metabolic effects underlying small-molecule drugs and drug candidates that impair TNBC pathogenicity by coupling drug screening with chemoproteomic and metabolomic profiling. In our first example, using isoTOP-ABPP platforms, we show here that licochalcone A impairs TNBC cell survival by >95% through inhibiting PTGR1. In our second example, using metabolomic platforms, we identify that deubiquitinase inhibitors also impair TNBC cell survival and that inhibiting these enzymes elevates AC levels by >60-fold to potentially impair cellular respiration and contribute to the viability impairments. Both PTGR1 inhibition and acyl carnitine-mediated respiratory impairments in TNBC cells represent novel metabolic modalities that affect TNBC pathogenicity. Future studies should focus on better understanding the inhibitory mechanisms of licochalcone A on PTGR1, developing potent and selective PTGR1 inhibitors, and ascertaining the role of PTGR1, leukotriene B4, and BLT1 signaling pathways on TNBC pathogenicity. Future studies also include understanding the mechanisms and molecular targets through which AC impairs mitochondrial respiration. Collectively, our data point to the utility of using chemoproteomic and metabolomic platforms to uncover novel metabolic regulators of cancer, toward developing novel cancer therapies.

METHODS

Materials. The anticancer compound library consisting of 424 compounds at 10 mM in DMSO was purchased from Selleck Chemicals. IAyne was obtained from CHESS Gmbh. Heavy and light TEV-biotin tags were synthesized per previously described methods.[29,40] Palmitoyl carnitine was obtained from Sigma-Aldrich and resuspended in deionized water to 100 mM stock. Lysophosphatidyl ethanolamine was obtained from Avanti Polar Lipids and resuspended in 2:1 chloroform/methanol to a 10 mM stock.

Cell Culture. The 231MFP cells were obtained from Professor Benjamin Cravatt and were generated from explanted tumor xenografts of MDA-MB-231 cells. HCC38, HCC70, and HEK293T cells were obtained from the American Type Culture Collection (ATCC). 231MFP cells were cultured in L15 (HyClone) medium containing 10% FBS, supplemented with 2% glutamine (200 mM stock), and maintained at 37 °C with 0% CO_2. HCC38 and HCC70 cells were cultured in RPMI (Gibco) medium containing 10% FBS, supplemented with 2% glutamine (200 mM stock), and maintained at 37 °C with 5% CO_2. HEK293T cells were cultured in DMEM (Corning) containing 10% FBS, supplemented with 2% glutamine (200 mM stock) and maintained at 37 °C with 5% CO_2.

Cellular Survival and Proliferation Studies. Cell survival assays were performed as previously described using Hoechst 33342 dye (Invitrogen) according to the manufacturer's protocol.[41] Cells were seeded into 96-well plates (40 000 cells) in a volume of 150 μL of serum-free media and allowed to adhere overnight. Once adhered, an additional 50 μL of serum-free media containing 1:250 dilution of 1000× compound stock in DMSO was added to each well and allowed to incubate for 48 h before fixation. The medium was removed from each well, and 100 μL of staining solution containing 10% formalin and Hoechst 33342 dye was added to each well and incubated for 15 min in the dark at RT. Staining solution was then removed, and 100 μL of PBS was added for imaging on a SpectraMax i3 fluorescent plate reader. Studies with HCC38 cells and HCC70 were also performed as above but were seeded with 20 000 and 30 000 cells, respectively. Cell proliferation assays were performed as above, but cells were seeded (20 000 for 231MFP cells) and treated in medium containing FBS.

IsoTOP-ABPP. IsoTOP-ABPP studies were done as previously reported.[27,29] Cell proteomes were prepared by sonicating harvested cell pellets in PBS, followed by centrifugation of proteomes at 1000g to remove any cell debris. Proteome samples diluted in PBS were treated

DOI: 10.1021/acschembio.6b01159
ACS Chem. Biol. XXXX, XXX, XXX−XXX

with licochalcone A or vehicle for 30 min at 37 °C. Then, IAyne labeling was performed for 1 h at RT. CuAAC was used by sequential addition of tris(2-carboxyethyl)phosphine (1 mM, Sigma), tris[(1-benzyl-1H-1,2,3-triazol-4-yl)methyl]amine (34 μM, Sigma), copper-(II) sulfate (1 mM, Sigma), and biotin-linker-azide, the linker functionalized with a TEV protease recognition sequence along with an isotopically light or heavy valine for treatment of control or treated proteome, respectively. After click reactions, proteomes were precipitated by centrifugation at 6500*g*, washed in ice-cold methanol, combined in a 1:1 control/treated ratio, washed again, then denatured and resolubilized by heating in 1.2% SDS/PBS to 80 °C for 5 min. Insoluble components were precipitated by centrifugation at 6500*g*, and soluble proteome was diluted in 5 mL of 0.2% SDS/PBS. Labeled proteins were enriched using avidin-agarose beads (170 μL beads/sample, Thermo Pierce) while rotating overnight at 4 °C. Probe-labeled proteins were enriched by washing three washes each with PBS and water, followed by resuspension of beads in 6 M urea/PBS and reduction of cysteines in TCEP (1 mM), alkylation with iodoacetamide (18 mM), washing and resuspension of beads in 2 M urea, and trypsinization overnight with 0.5 μg/μL sequencing grade trypsin (Promega). Tryptic peptides were eluted off. Beads were then further washed in PBS and water, washed in TEV buffer solution (water, TEV buffer, 100 mM dithiothreitol), and resuspended in buffer with Ac-TEV protease and incubated overnight. Peptides were diluted in water and acidified with formic acid (1.2 M), and tryptic peptides were stored at −80 °C until MS analysis.

MS Analysis. Total peptides eluted from TEV protease release of probe-modified peptides were pressure-loaded onto 250 μm inner diameter fused silica capillary tubing packed with 4 cm of Aqua C18 reverse-phase resin (Phenomenex # 04A-4299) which was previously equilibrated. This capillary tubing containing the loaded peptides was then attached using a MicroTee PEEK 360 mm fitting (Thermo Fisher Scientific #p-888) to a nanospray column consisting of 10 cm of C18 reverse-phase and 3 cm of strong-cation exchange resin. Samples were analyzed using an Q Exactive Plus mass spectrometer (Thermo Fisher Scientific) using a Multidimensional Protein Identification Technology (MudPIT) program, using 0%, 25%, 50%, 80%, and 100% salt bumps of 500 mM ammonium acetate and using a gradient of 5−55% buffer B in buffer A (buffer A. 95:5 water/acetonitrile, 0.1% formic acid; buffer B. 80:20 acetonitrile/water, 0.1% formic acid). Data were collected in data-dependent acquisition mode with dynamic exclusion enabled (60 s). One full MS (MS1) scan (400−1800 m/z) was followed by 15 MS2 scans of the most abundant ions. Heated capillary temperature and nanospray voltage were 200 °C and 2.75 kV, respectively.

Data were extracted in the form of MS1 and MS2 files using Raw Extractor 1.9.9.2 (Scripps Research Institute) and searched against the Uniprot human database using ProLuCID search methodology in IP2 v.3 (Integrated Proteomics Applications, Inc.).[42] Cysteine residues were searched with a static carboxyaminomethylation (+57.02146) modification for up to two differential modifications for methionine oxidation and either the light or heavy TEV tags (+464.28596 or +470.29977, respectively). Peptides were required to have at least one tryptic end and to contain the TEV modification. Data were filtered through DTASelect to ensure a peptide false-positive less than 1%.

Gel-Based ABPP. Gel-based ABPP methods were performed as previously described.[43] Recombinant PTGR1 (0.1 μg) protein (Origene) was pretreated with DMSO or licochalcone A, respectively, for 1 h at 37 °C in an incubation volume of 50 μL of PBS and was subsequently treated with IAyne (1 μM final concentration) for 30 min at 37 °C. CuAAC was performed to append rhodamine-azide onto IAyne probe-labeled proteins. The samples were separated by SDS/PAGE and scanned using a ChemiDoc MP (Bio-Rad Laboratories, Inc.). Inhibition of target labeling was assessed by densitometry using ImageStudio Light software.

Metabolomic Profiling. Metabolomic profiling was performed as previously reported.[41,44] For metabolomic profiling, 2 million cells were seeded in complete media and allowed to adhere overnight. They were then washed with PBS and refed with serum-free media containing 10 μM of compound in DMSO or DMSO vehicle control at 0.1% DMSO final concentration for 6 h. The cells were harvested and flash-frozen, and metabolomes were extracted in 3 mL of 2:1 chloroform/methanol and 1 mL of PBS with inclusion of internal standards dodecylglycerol (10 nmol, Santa Cruz Biotechnology) and pentadecanoic acid (10 nmol, Sigma-Aldrich). Organic and aqueous layers were separated by centrifugation at 1000*g* for 5 min, and the organic layer was collected, dried under a stream of nitrogen, and dissolved in 120 μL of chloroform. A 10 μL aliquot of the 120 μL sample in chloforom was then injected into an Agilent 6430 QQQ-LC/MS/MS. Metabolomes were separated using reverse-phase chromatography with a Luna C5 column (50 mm × 4.6 mm with 5 μm diameter particles, Phenomenex) using previously reported methods.[41,44]

Metabolites were identified by single-reaction monitoring of the transition from precursor to product ions at associated optimized collision energies and retention times as previously described.[41,44] Metabolites were quantified by integrating the area under the curve and then normalized to internal standard values. Metabolite levels are expressed as relative abundances as compared to controls.

PTGR1 Knockdown. Targets were knocked down stably with shRNA as previously described.[41,44] shControl (targeting GFP) or shPTGR1 constructs (Sigma) were transfected into HEK293T (ATCC) cells alongside lentiviral vectors using lipofectamine 2000 (Thermo Fisher Scientific). Lentivirus was collected from filtered cultured medium 48 h post-transfection and used to infect the target cancer cell line with Polybrene (0.01 mg mL^{-1}). Target cells were selected over 3 days with 1 mg mL^{-1} puromycin. The short hairpin sequences for the generation of PTGR1 knockdown lines were

shPTGR1−1: CCGGCTTGGATTTGATGTCGTCTT-TCTCGAGAAAGACGACATCAAATCCAAGTTTTT

shPTGR1−2: CCGGCTATCCTACTAATAGTGACT-TCTCGAGAAGTCACTATTAGTAGGATAGTTTTT

shPTGR1−3: CCGGGCCTACTTTGGCCTACTTGA-ACTCGAGTTCAAGTAGGCCAAAGTAGGCTTTTT

control shRNA against GFP: GCAAGCTGACCCTGAAGTTCAT.

Knockdown was confirmed by qPCR.

qPCR. qPCR was performed using the manufacturer's protocol for Fisher Maxima SYBR Green. Primer sequences are as follows:

PTGR1 forward: AGCACTTTGTTGGCTATCCTAC

PTGR1 reverse: CCCCATCATTGTATCACCTTCC

Cyclophilin forward: CCCACCGTGTTCTTCGACATT

Cyclophilin reverse: GGACCCGTATGCTTTAGGATGA

Cellular Respiration Measurements. 231MFP cells were seeded at 50 000 cells/well in an XF24 cell culture microplate (Seahorse Bioscience) and analyzed the following day. On the day of analysis, cells were washed once with Seahorse respiration buffer made up of XF base medium minimal DMEM containing 25 mM glucose and 5 mM sodium pyruvate with the pH adjusted to 7.4. The cells were then placed in 0.5 mL of Seahorse respiration buffer and incubated in a CO_2-free incubator for 1 h. The 10× port injection solutions, in Seahorse respiration buffer all pH adjusted to 7.4, were prepared as follows (final concentrations in parentheses): port A, 10 μM oligomycin (1 μM final); port B, 1 mM palmitoyl carnitine (100 μM final) or 100 μM WP1130 (10 μM final); port C, 3 μM FCCP (0.3 μM final); port D, 5 μM rotenone and 5 μM antimycin A (0.5 μM final). The Seahorse program ran as follows: basal measurement, three cycles; inject port A (oligomycin), three cycles; inject port B (compounds), three cycles; inject port C (FCCP), three cycles; inject port D (rotenone and antimycin A), three cycles. Each cycle consisted of mix for 3 min, wait for 2 min, measure for 3 min.

■ ASSOCIATED CONTENT

Supporting Information

The Supporting Information is available free of charge on the ACS Publications website at DOI: 10.1021/acschembio.6b01159.

Figures S1−S4 and descriptions of Tables S1−S3 (PDF)

Compounds, targets, and screen data (XLSX)

DOI: 10.1021/acschembio.6b01159
ACS Chem. Biol. XXXX, XXX, XXX−XXX

IsoTOP-ABPP analysis of licochalcone A in 231MFP breast cancer cells (XLSX)

Metabolomic profiling of drug responses in 231MFP breast cancer cells (XLSX)

AUTHOR INFORMATION

Corresponding Author

*E-mail: dnomura@berkeley.edu.

ORCID

Daniel K. Nomura: 0000-0003-1614-8360

Notes

The authors declare no competing financial interest.

ACKNOWLEDGMENTS

We thank the members of the Nomura Research Group for critical reading of the manuscript. This work was supported by grants from the National Institutes of Health (R01CA172667 for D.K.N., L.S.R.), American Cancer Society Research Scholar Award (RSG14-242-01-TBE for D.K.N., L.S.R.), Department of Defense Breast Cancer Research Program Breakthroughs Award (CDMRP W81XWH-15-1-0050), and National Science Foundation Graduate Fellowship (L.S.R.).

REFERENCES

(1) NIH-SEER database. https://seer.cancer.gov/.

(2) Li, Z., and Kang, Y. (2016) Emerging therapeutic targets in metastatic progression: A focus on breast cancer. *Pharmacol. Ther. 161*, 79.

(3) Dietze, E. C., Sistrunk, C., Miranda-Carboni, G., O'Regan, R., and Seewaldt, V. L. (2015) Triple-negative breast cancer in African-American women: disparities versus biology. *Nat. Rev. Cancer 15*, 248–254.

(4) Zeichner, S. B., Terawaki, H., and Gogineni, K. (2016) A Review of Systemic Treatment in Metastatic Triple-Negative Breast Cancer. *Breast Cancer: Basic Clin. Res. 10*, 25–36.

(5) Polyak, K., and Weinberg, R. A. (2009) Transitions between epithelial and mesenchymal states: acquisition of malignant and stem cell traits. *Nat. Rev. Cancer 9*, 265–273.

(6) Breast Cancer Treatment, Natl. Cancer Inst. PDQ Cancer Info Summary. https://www.cancer.gov/types/breast/patient/breast-treatment-pdq.

(7) Benjamin, D. I., Cravatt, B. F., and Nomura, D. K. (2012) Global profiling strategies for mapping dysregulated metabolic pathways in cancer. *Cell Metab. 16*, 565–577.

(8) Bianchini, G., Balko, J. M., Mayer, I. A., Sanders, M. E., and Gianni, L. (2016) Triple-negative breast cancer: challenges and opportunities of a heterogeneous disease. *Nat. Rev. Clin. Oncol. 13*, 674–690.

(9) Dar, A. A., Goff, L. W., Majid, S., Berlin, J., and El-Rifai, W. (2010) Aurora Kinases' Inhibitors – Rising Stars in Cancer Therapeutics? *Mol. Cancer Ther. 9*, 268.

(10) Singh, J., Novik, Y., Stein, S., Volm, M., Meyers, M., Smith, J., Omene, C., Speyer, J., Schneider, R., Jhaveri, K., Formenti, S., Kyriakou, V., Joseph, B., Goldberg, J. D., Li, X., Adams, S., and Tiersten, A. (2014) Phase 2 trial of everolimus and carboplatin combination in patients with triple negative metastatic breast cancer. *Breast Cancer Res. BCR 16*, R32.

(11) Gomez, H. L., Philco, M., Pimentel, P., Kiyan, M., Monsalvo, M. L., Conlan, M. G., Saikali, K. G., Chen, M. M., Seroogy, J. J., Wolff, A. A., and Escandon, R. D. (2012) Phase I dose-escalation and pharmacokinetic study of ispinesib, a kinesin spindle protein inhibitor, administered on days 1 and 15 of a 28-day schedule in patients with no prior treatment for advanced breast cancer. *Anti-Cancer Drugs 23*, 335–341.

(12) Trinh, X. B., Sas, L., Van Laere, S. J., Prové, A., Deleu, I., Rasschaert, M., Van de Velde, H., Vinken, P., Vermeulen, P. B., Van Dam, P. A., Wojtasik, A., De Mesmaeker, P., Tjalma, W. A., and Dirix, L. Y. (2012) A phase II study of the combination of endocrine treatment and bortezomib in patients with endocrine-resistant metastatic breast cancer. *J. Clin. Oncol. 27*, 657–663.

(13) Von Hoff, D. D., Taylor, C., Rubin, S., Cohen, J., and Garland, L. (2004) A Phase I and pharmacokinetic study of HMN-214, a novel oral polo-like kinase inhibitor, in patients with advanced solid tumors. *J. Clin. Oncol. Off. J. Am. Soc. Clin. Oncol. 22*, 3034.

(14) Claude-Taupin, A., Boyer-Guittaut, M., Delage-Mourroux, R., and Hervouet, E. (2015) Use of epigenetic modulators as a powerful adjuvant for breast cancer therapies. *Methods Mol. Biol. 1238*, 487–509.

(15) Xiao, Z., Zhang, P., and Ma, L. (2016) The role of deubiquitinases in breast cancer. *Cancer Metastasis Rev. 35*, 589.

(16) Alasmael, N., Mohan, R., Meira, L. B., Swales, K. E., and Plant, N. J. (2016) Activation of the Farnesoid X-receptor in breast cancer cell lines results in cytotoxicity but not increased migration potential. *Cancer Lett. 370*, 250–259.

(17) Rafi, M. M., Rosen, R. T., Vassil, A., Ho, C. T., Zhang, H., Ghai, G., Lambert, G., and DiPaola, R. S. (2000) Modulation of bcl-2 and cytotoxicity by licochalcone-A, a novel estrogenic flavonoid. *Anticancer Res. 20*, 2653–2658.

(18) Chen, L. C., Rosen, L. S., Iyengar, T., Goldman, J. W., Savage, R., Kazakin, J., Chan, T. C. K., Schwartz, B. E., Abbadessa, G., and Von Hoff, D. D. (2011) First-in-human study with ARQ 621, a novel inhibitor of Eg5: Final results from the solid tumors cohort. *J. Clin. Oncol. 29*, 3076.

(19) Almahariq, M., Chao, C., Mei, F. C., Hellmich, M. R., Patrikeev, I., Motamedi, M., and Cheng, X. (2015) Pharmacological inhibition and genetic knockdown of exchange protein directly activated by cAMP 1 reduce pancreatic cancer metastasis in vivo. *Mol. Pharmacol. 87*, 142–149.

(20) Bortolotto, L. F. B., Barbosa, F. R., Silva, G., Bitencourt, T. A., Beleboni, R. O., Baek, S. J., Marins, M., and Fachin, A. L. (2016) Cytotoxicity of trans-chalcone and licochalcone A against breast cancer cells is due to apoptosis induction and cell cycle arrest. *Biomed. Pharmacother. 85*, 425.

(21) Hu, J., and Liu, J. (2016) Licochalcone A Attenuates Lipopolysaccharide-Induced Acute Kidney Injury by Inhibiting NF-κB Activation. *Inflammation 39*, 569–574.

(22) Tsai, J.-P., Lee, C.-H., Ying, T.-H., Lin, C.-L., Lin, C.-L., Hsueh, J.-T., and Hsieh, Y.-H. (2015) Licochalcone A induces autophagy through PI3K/Akt/mTOR inactivation and autophagy suppression enhances Licochalcone A-induced apoptosis of human cervical cancer cells. *Oncotarget 6*, 28851–28866.

(23) Yang, X., Jiang, J., Yang, X., Han, J., and Zheng, Q. (2016) Licochalcone A induces T24 bladder cancer cell apoptosis by increasing intracellular calcium levels. *Mol. Med. Rep. 14*, 911–919.

(24) Yadav, N., Dixit, S. K., Bhattacharya, A., Mishra, L. C., Sharma, M., Awasthi, S. K., and Bhasin, V. K. (2012) Antimalarial activity of newly synthesized chalcone derivatives in vitro. *Chem. Biol. Drug Des. 80*, 340–347.

(25) Chularojanamontri, L., Tuchinda, P., Kulthanan, K., Varothai, S., and Winayanuwattikun, W. (2016) A double-blinded, randomized, vehicle-controlled study to access skin tolerability and efficacy of an anti-inflammatory moisturizer in treatment of acne with 0.1% adapalene gel. *J. Dermatol. Treat. 27*, 140–145.

(26) Shannon, D. A., and Weerapana, E. (2015) Covalent protein modification: the current landscape of residue-specific electrophiles. *Curr. Opin. Chem. Biol. 24*, 18–26.

(27) Backus, K. M., Correia, B. E., Lum, K. M., Forli, S., Horning, B. D., González-Páez, G. E., Chatterjee, S., Lanning, B. R., Teijaro, J. R., Olson, A. J., Wolan, D. W., and Cravatt, B. F. (2016) Proteome-wide covalent ligand discovery in native biological systems. *Nature 534*, 570–574.

DOI: 10.1021/acschembio.6b01159
ACS Chem. Biol. XXXX, XXX, XXX–XXX

(28) Wang, C., Weerapana, E., Blewett, M. M., and Cravatt, B. F. (2014) A chemoproteomic platform to quantitatively map targets of lipid-derived electrophiles. *Nat. Methods 11*, 79−85.
(29) Weerapana, E., Wang, C., Simon, G. M., Richter, F., Khare, S., Dillon, M. B. D., Bachovchin, D. A., Mowen, K., Baker, D., and Cravatt, B. F. (2010) Quantitative reactivity profiling predicts functional cysteines in proteomes. *Nature 468*, 790−795.
(30) Roberts, A. M., Ward, C. C., and Nomura, D. K. (2016) Activity-based protein profiling for mapping and pharmacologically interrogating proteome-wide ligandable hotspots. *Curr. Opin. Biotechnol. 43*, 25−33.
(31) Mesa, J., Alsina, C., Oppermann, U., Parés, X., Farrés, J., and Porté, S. (2015) Human prostaglandin reductase 1 (PGR1): Substrate specificity, inhibitor analysis and site-directed mutagenesis. *Chem.-Biol. Interact. 234*, 105−113.
(32) Huang, X., Zhou, W., Zhang, Y., and Liu, Y. (2016) High Expression of PTGR1 Promotes NSCLC Cell Growth via Positive Regulation of Cyclin-Dependent Protein Kinase Complex. *BioMed Res. Int. 2016*, 5230642.
(33) Xue, L., Zhu, Z., Wang, Z., Li, H., Zhang, P., Wang, Z., Chen, Q., Chen, H., and Chong, T. (2016) Knockdown of prostaglandin reductase 1 (PTGR1) suppresses prostate cancer cell proliferation by inducing cell cycle arrest and apoptosis. *BioSci. Trends 10*, 133−139.
(34) Jeon, W.-K., Choi, J., Park, S. J., Jo, E. J., Lee, Y. K., Lim, S., Kim, J.-H., Letterio, J. J., Liu, F., Kim, S.-J., and Kim, B.-C. (2015) The proinflammatory LTB4/BLT1 signal axis confers resistance to TGF-β1-induced growth inhibition by targeting Smad3 linker region. *Oncotarget 6*, 41650−41666.
(35) Yue, W. W., Shafqat, N., Krojer, T., Pike, A. C. W., Von Delft, F., Sethi, R., Savitsky, P., Johansson, C., Arrowsmith, C., Weigelt, J., Edwards, A., Bountra, C., and Oppermann, U. Crystal structure of human leukotriene B4 12-hydroxydehydrogenase in complex with NADP and raloxifene. RCS Protein Data Bank 2Y05. DOI 10.2210/pdb2y05/pdb.
(36) Rasmussen, B. B., and Wolfe, R. R. (1999) Regulation of fatty acid oxidation in skeletal muscle. *Annu. Rev. Nutr. 19*, 463−484.
(37) Yamada, K. A., McHowat, J., Yan, G. X., Donahue, K., Peirick, J., Kléber, A. G., and Corr, P. B. (1994) Cellular uncoupling induced by accumulation of long-chain acylcarnitine during ischemia. *Circ. Res. 74*, 83−95.
(38) Wajner, M., and Amaral, A. U. (2016) Mitochondrial dysfunction in fatty acid oxidation disorders: insights from human and animal studies. *Biosci. Rep. 36*, e00281.
(39) Yamada, K. A., Kanter, E. M., and Newatia, A. (2000) Long-chain acylcarnitine induces Ca2+ efflux from the sarcoplasmic reticulum. *J. Cardiovasc. Pharmacol. 36*, 14−21.
(40) Weerapana, E., Speers, A. E., and Cravatt, B. F. (2007) Tandem orthogonal proteolysis-activity-based protein profiling (TOP-ABPP)—a general method for mapping sites of probe modification in proteomes. *Nat. Protoc. 2*, 1414−1425.
(41) Louie, S. M., Grossman, E. A., Crawford, L. A., Ding, L., Camarda, R., Huffman, T. R., Miyamoto, D. K., Goga, A., Weerapana, E., and Nomura, D. K. (2016) GSTP1 Is a Driver of Triple-Negative Breast Cancer Cell Metabolism and Pathogenicity. *Cell Chem. Biol. 23*, 567−578.
(42) Xu, T., Park, S. K., Venable, J. D., Wohlschlegel, J. A., Diedrich, J. K., Cociorva, D., Lu, B., Liao, L., Hewel, J., Han, X., Wong, C. C. L., Fonslow, B., Delahunty, C., Gao, Y., Shah, H., and Yates, J. R. (2015) ProLuCID: An improved SEQUEST-like algorithm with enhanced sensitivity and specificity. *J. Proteomics 129*, 16−24.
(43) Medina-Cleghorn, D., Bateman, L. A., Ford, B., Heslin, A., Fisher, K. J., Dalvie, E. D., and Nomura, D. K. (2015) Mapping Proteome-Wide Targets of Environmental Chemicals Using Reactivity-Based Chemoproteomic Platforms. *Chem. Biol. 22*, 1394−1405.
(44) Benjamin, D. I., Cozzo, A., Ji, X., Roberts, L. S., Louie, S. M., Mulvihill, M. M., Luo, K., and Nomura, D. K. (2013) Ether lipid generating enzyme AGPS alters the balance of structural and signaling lipids to fuel cancer pathogenicity. *Proc. Natl. Acad. Sci. U. S. A. 110*, 14912−14917.

DOI: 10.1021/acschembio.6b01159
ACS Chem. Biol. XXXX, XXX, XXX−XXX